

Experimental electric field and dielectric tissue property mapping using a regularized CSI-EPT reconstruction method

Edmond Balidemaj¹, Johan Trinks¹, Rob F. Remis², Hans Crezee¹, Astrid van Lier³, Aart J. Nederveen⁴, and Cornelis A.T. van den Berg³

¹Radiotherapy, Academic Medical Center, Amsterdam, Netherlands, ²Technical University Delft, Delft, Netherlands, ³UMC Utrecht, Utrecht, Netherlands,

⁴Academic Medical Center, Amsterdam, Netherlands

Introduction & Theory: Electric Properties Tomography (EPT) [1] and local Maxwell Tomography [2] are MR-based techniques to reconstruct dielectric tissue profiles (conductivity σ and permittivity ϵ_r) from measured B_1^+ data. These techniques are based on Maxwell's equations in differential or integral form and assume piecewise constant media. This assumption may result in significant reconstruction errors especially near interfaces between different tissue types and the method may suffer from instabilities, since local differential operators act on measured and noisy data. Recently, we have proposed to apply the so-called Contrast Source Inversion method using B_1^+ data as measured in a typical MRI setting. This method does not assume piecewise constant media and works with global integral representations for the fields. In this work we show how the effects of noise can be suppressed in CSI-EPT by introducing a multiplicative regularization term in the objective functional. Furthermore, we extend our reconstruction algorithm such that multiple B_1^+ data sets for different shim (antenna phase) settings can be simultaneously included in the iterative CSI-EPT process leading to an overall improvement of the reconstructed dielectric values. Furthermore, CSI-EPT reconstructs the electrical field and is therefore a promising method to determine SAR deposition.

Materials & Methods: The CSI-EPT method is based on two domain integral representations of the electromagnetic field. The first integral representation (1), known as the *data equation*, relates the measured field \mathbf{f} to the contrast source \mathbf{w} via the electric-current to magnetic field

Green's tensor \mathbf{G}^{HJ} of the background medium. The contrast source $\mathbf{w}(\mathbf{x}) = \chi(\mathbf{x})\mathbf{E}(\mathbf{x})$ consists of the product of the unknown dielectric profile function $\chi(\mathbf{x}) = \epsilon_r(\mathbf{x}) - 1 - j\sigma(\mathbf{x})/(\omega\epsilon_0)$ and the unknown total electric field \mathbf{E} . Although we do not know this field, we do know that it must satisfy Maxwell's equations. In integral form, this amounts to requiring that the electric field satisfies the so-called *object equation* (2). Eq. (2) therefore acts as a constraint for the data equation. \mathbf{G}^{EJ} is the electric-current to electric field Green's tensor in free space and \mathbf{E}^{inc} is the electric field inside an empty coil. In [3], we update the contrast source and contrast function in an iterative fashion by minimizing an objective function $F(\mathbf{w}, \chi) = F_{\text{data}}(\mathbf{w}) + F_{\text{object}}(\mathbf{w}, \chi)$, where $F_{\text{data}}(\mathbf{w})$ and $F_{\text{object}}(\mathbf{w}, \chi)$ measure the discrepancy in satisfying the Eq. (1) and (2), respectively. To handle noisy B_1^+ data, we now include a *multiplicative* total variation (TV) regularization term and minimize the regularized objective function

$$\mathbf{f}(\mathbf{x}) = \int_{\mathbf{x}' \in D} \mathbf{G}^{\text{HJ}}(\mathbf{x}, \mathbf{x}') \mathbf{w}(\mathbf{x}') dV \quad (1) \quad F(\mathbf{w}, \chi) = [F_{\text{data}}(\mathbf{w}) + F_{\text{object}}(\mathbf{w}, \chi)] F_{\text{TV}}(\chi). \quad (2)$$

$$\mathbf{E}(\mathbf{x}) - \int_{\mathbf{x}' \in D} \mathbf{G}^{\text{EJ}}(\mathbf{x}, \mathbf{x}') \mathbf{w}(\mathbf{x}') dV = \mathbf{E}^{\text{inc}}(\mathbf{x}) \quad (2)$$

The regularization term $F_{\text{TV}}(\chi)$ ensures that rapid variations due to noisy data are suppressed during the updating procedure. Furthermore, data obtained for different phase settings (n) of the transmit coil can be handled simultaneously by minimizing the total objective function $F^{\text{tot}}(\mathbf{w}, \chi) = \sum_n [F_{\text{data}}(\mathbf{w}) + F_{\text{object}}(\mathbf{w}, \chi)] F_{\text{TV}}(\chi)$, which consists of a summation of

regularized objective functions for each phase setting separately. The algorithm yields the contrast function χ and contrast source \mathbf{w} and since $\mathbf{w}(\mathbf{x}) = \chi(\mathbf{x})\mathbf{E}(\mathbf{x})$, we have essentially reconstructed the electric field as well. Mathematical details about updating with and without TV regularization can be found in [4]. The B_1^+ amplitude [5] and transceive phase [6] were measured (3T) for a pelvic-sized phantom [7].

Results & Discussion: In Fig. 1 the actual σ and ϵ_r profiles of a female pelvis model (Ella, ITIS) are shown. The corresponding B_1^+ fields are computed by using 16 RF line sources (driven at 128MHz) located symmetrically around the object. This field (contaminated with Gaussian noise, SNR 20) serves as an input for CSI-EPT. Here we have assumed that perfect B_1^+ transmit phase is available [2] without receive phase contamination. In Fig. 1 (2nd col.) the results are clearly contaminated by noise when applying standard CSI-EPT reconstruction (1000 iterations, computation time: 30 sec). Applying TV regularization, the reconstructed profiles are dramatically improved (Fig. 1 3rd col), where quadrature drive phase setting was used for excitation of B_1^+ fields. We do observe, however, that the reconstructions are still noisy on the diagonal where the main longitudinal electric fields cancel for quadrature drive. By changing the phase settings the electric field interference pattern changes and the corresponding reconstructions change accordingly (Fig. 1. 4th col). The destructive interference problem can be circumvented, however, by combining the different phase sets and using the total objective function $F^{\text{tot}}(\mathbf{w}, \chi)$, see Fig. 1 (5th col). The reconstructions show a clear overall improvement and interference problems are no longer observed. The reconstructed values of several tissue types, listed in Table I, are in good agreement with the true values. In Fig. 2 (left) the phantom model ($\sigma_{\text{in}}=0.64$, $\sigma_{\text{out}}=0.44$ [S/m]) and E-field amplitude (FDTD simulations) are shown. In Fig. 2 (right) the reconstructed σ ($\sigma_{\text{in}}=0.64 \pm 0.11$, $\sigma_{\text{out}}=0.46 \pm 0.6$ [S/m]) values based on measured B_1^+ fields are shown. The reconstructed E-field amplitude is in good agreement with the E-field based on FDTD simulation.

Conclusions: We have presented a new noise-robust approach to retrieve dielectric maps from B_1^+ data based on the recently introduced CSI-EPT method. The presented results demonstrate the ability of CSI-EPT to reconstruct dielectric profiles from contaminated noisy B_1^+ data by employing total variation regularization. Furthermore, the use of more than one B_1^+ field distributions in the algorithm has been implemented and has shown to improve the reconstructed dielectric profiles for in vivo simulations and pelvic-sized phantom experiments. This method can be extended to 3D problems as shown in several CSI studies [4].

References [1] Katscher *et al.*, IEEE 28:1365-75, 2009. [2] Sodickson, ISMRM 2013, 4175 [3] Balidemaj, ICEAA 2013, IEEE p.668 - 671. [4] Van den Berg, P. M., PIER 34, 189-218, 2001. [5] Yamykh, MRM 57:192-200, 2007. [6] Van Lier, ISMRM p.125, 2011. [7] Balidemaj, ISMRM 2013 p.4178.

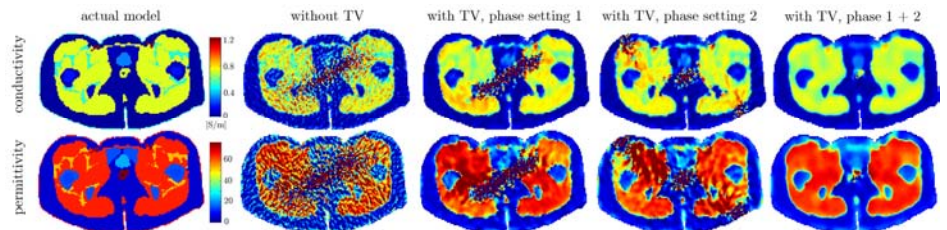


Fig 1. Original σ and ϵ_r profiles and reconstructed profiles obtained without TV regularization (2nd column), with TV with various phase settings (3rd and 4th column) and combined setting 1 and 2 (5th column).

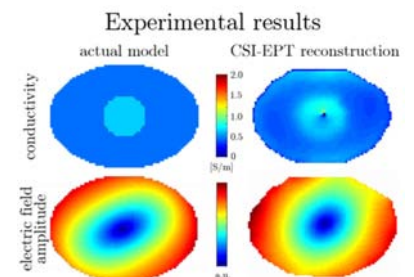


Fig 2. Phantom model σ and E-field amplitude (left) and reconstructed σ and E-field based on regularized CSI-EPT.

Table I. True and reconstructed values of several tissue types

	Actual pelvis model		Reconstructed values of 5 th column of Fig 1.	
	σ [S/m]	ϵ_r	σ [S/m]	ϵ_r
Muscle	0.7192	63.4950	0.68 ± 0.09	60.45 ± 8.46
Fat	0.0369	5.9215	0.10 ± 0.09	11.00 ± 8.42
Bladder	0.2980	21.8610	0.24 ± 0.06	17.56 ± 2.46